INTERNATIONAL JOURNAL OF ROBUST AND NONLINEAR CONTROL
Int. J. Robust Nonlinear Control 2010; **20**:1017–1026
Published online 3 November 2009 in Wiley InterScience (www.interscience.wiley.com). DOI: 10.1002/rnc.1528

Analysis and extension of a biochemical network model using robust control theory

J.-S. Kim[1], N. V. Valeyev[2], I. Postlethwaite[2], P. Heslop-Harrison[2,3], K.-H. Cho[4,*,†] and D. G. Bates[2,‡,§]

[1]*Department of Control and Instrumentation Engineering, Seoul National University of Technology, 172 Gongneung 2-dong, Nowon-gu, Seoul 139-743, Korea*
[2]*Systems Biology Lab, Department of Engineering, University of Leicester, University Road, Leicester LE1 7RH, U.K.*
[3]*Department of Biology, University of Leicester, University Road, Leicester LE1 7RH, U.K.*
[4]*Department of Bio and Brain Engineering, Korea Advanced Institute of Science and Technology (KAIST), Daejeon 305-701, Korea*

SUMMARY

Mathematical models of biological processes which have been observed *in vivo* to be highly robust to intracellular and environmental variations should themselves display appropriate levels of robustness when analysed *in silico*. This paper uses techniques from robust control theory to analyse and extend a mathematical model of the interacting proteins underlying adenosine 3′, 5′-cyclic monophosphate (cAMP) oscillations in aggregating *Dictyostelium* cells. Starting with a previously proposed 'minimal' model, we show how robustness analysis using the structured singular value can identify points of structural fragility in the network. By combining these results with insights from recent results from the experimental literature, we show how the original model can be augmented with some important additional modules, comprising networks involving IP_3 and Ca^{2+}. By analysing the robustness of our new extended model, we are able to show that dynamic interactions between the different modules play a pivotal role in generating robust cAMP oscillations; thus, significantly improving our understanding of the design principles underlying this complex biological system. Copyright © 2009 John Wiley & Sons, Ltd.

Received 31 March 2009; Revised 10 July 2009; Accepted 20 September 2009

KEY WORDS: robustness analysis; structured singular value; *Dictyostelium*; systems biology

1. INTRODUCTION

Over the last decade of research in the field of Systems Biology, the concept of robustness has emerged as a

*Correspondence to: K.-H. Cho, Department of Bio and Brain Engineering, Korea Advanced Institute of Science and Technology (KAIST), Daejeon 305-701, Korea.
†E-mail: ckh@kaist.ac.kr, URL: http://sbie.kaist.ac.kr/
‡Correspondence to: D.G. Bates, Systems Biology Lab, Department of Engineering, University of Leicester, University Road, Leicester LE1 7RH, U.K.
§E-mail: dgb3@leicester.ac.uk

Contract/grant sponsor: BBSRC; contract/grant number: BB/D015340/1
Contract/grant sponsor: BRL (Basic Research Laboratory); contract/grant number: 2009-0086964
Contract/grant sponsor: Systems Biology; contract/grant number: 20090065567
Contract/grant sponsor: Nuclear Research; contract/grant number: M20708000001-07B0800-00110
Contract/grant sponsor: 21C Frontier Microbial Genomics and Application Center Program; contract/grant number: MG08-0205-4-0
Contract/grant sponsor: WCU; contract/grant number: R32-2008-000-10218-0
Contract/grant sponsor: Systems biology infrastructure establishment grant

key organizing principle of biological systems. One of the main ways in which many organisms ensure robust functionality under various chemical, biophysical, and environmental variations is via feedback control [1–7]. It is thus not surprising that such systems have recently attracted a great deal of attention from control engineers, who since the emergence of robust control theory have developed many powerful techniques for analysing the robustness of complex systems [8–10]. An important application of such techniques is to address the problem of model validation [11, 12]—if a proposed model of a biological system can be shown to lack the type or level of robustness demonstrated by the organism *in vivo*, then this can indicate that the model requires modification or further development to adequately explain the underlying biological phenomena.

Dictyostelium discoideum are social amoebae that normally live in forest soil, where they feed on bacteria [13]. Under conditions of starvation, *Dictyostelium* cells begin a programme of development during which they aggregate to eventually form spores atop a stalk of vacuolated cells. At the beginning of this process the amoebae become chemotactically sensitive to adenosine 3′, 5′-cyclic monophosphate (cAMP), and after about 6 h they acquire competence to relay cAMP signals. After 8 h, a few pacemaker cells start to emit cAMP periodically. Surrounding cells move towards the cAMP source and relay the cAMP signal to more distant cells. Eventually, the entire population collects into mound-shaped aggregates containing up to 10^5 cells. The processes involved in cAMP signalling in *Dictyostelium* are mediated by a family of cell surface cAMP receptors (cARs) that act on a specific heterotrimeric guanine nucleotide-binding proteins (G protein) to stimulate actin polymerization, activation of adenylyl cyclase (ACA) and guanylyl cyclase, and a number of other responses. Most of the components of these pathways have mammalian counterparts, and much effort has been devoted in recent years to the study of signal transduction mechanisms in these simple microorganisms, with the eventual aim of improving understanding of defects in these pathways which may lead to disease in humans [13–15].

In [13], a mathematical model was proposed for the network of interacting proteins involved in generating cAMP oscillations during the early development stage of *Dictyostelium* aggregation, and the dynamics of the model were claimed to be highly robust when subjected to trial-and-error variations of one kinetic parameter at a time. More systematic robustness analyses of this model published in [3, 16], however, revealed a surprising lack of robustness in the model's dynamics to a set of extremely small perturbations in its parameter space. Since the cAMP oscillations observed *in vivo* are clearly very robust to wide variations in these parameters, this result could be interpreted as casting some doubt on the validity of the model. On the other hand, there is strong experimental evidence to support each of the stages and interconnections in the proposed network, and the 'nominal' model's dynamics show an excellent match to the data. Subsequent studies showed that both intracellular stochastic noise and extracellular cell-to-cell synchronization acted to improve the robustness of the proposed model [17], but still failed to generate the levels of robustness which would be expected based on the reported experimental data. In this paper, we show how an analysis of the structural robustness of the model, using the approach of [12], allows us to pinpoint the parts of the network exhibiting extreme fragility. Informed by recent results from the experimental literature, we are then able to extend the model to include additional modules that interact with the original model at exactly these fragile points in the network. The resulting dramatic improvement in robustness of the extended model clearly reveals the crucial role played by dynamic interactions between (apparently redundant) calcium (Ca^{2+}), inositol trisphosphate (IP_3) and G protein-dependent modules in allowing the maintenance of stable cAMP oscillations for an individual cell even in the absence of strong extracellular cAMP waves.

2. STRUCTURAL ROBUSTNESS ANALYSIS OF A MODEL OF cAMP OSCILLATIONS IN DICTYOSTELIUM

In this section, we briefly introduce the 'minimal' mathematical model for the network of proteins underlying cAMP oscillations in aggregating *Dictyostelium* cells. We then show how fragile points in the network may be identified using tools from robust control theory.

DOI: 10.1002/rnc

2.1. A mathematical model of cAMP oscillations in Dictyostelium

In [13], a network of interacting proteins was proposed to explain the generation of stable oscillations in cAMP (and a number of other molecular species) during the early stages of *Dictyostelium* aggregation. The dynamics of this network can be represented using the following set of nonlinear differential equations [13]:

$$\begin{aligned}
\dot{x}_1 &= k_1 x_7 - k_2 x_1 x_2 \\
\dot{x}_2 &= k_3 x_5 - k_4 x_2 \\
\dot{x}_3 &= k_5 x_7 - k_6 x_2 x_3 \\
\dot{x}_4 &= k_7 - k_8 x_3 x_4 \\
\dot{x}_5 &= k_9 x_1 - k_{10} x_4 x_5 \\
\dot{x}_6 &= k_{11} x_1 - k_{12} x_6 \\
\dot{x}_7 &= k_{13} x_6 - k_{14} x_7
\end{aligned} \tag{1}$$

where x_1 is ACA, x_2 is PKA (protein kinase A), x_3 is ERK2 (mitogen-activated protein kinase), x_4 is intracellular RegA (internal cAMP phosphodiesterase), x_5 is internal cAMP, x_6 is external cAMP, x_7 is the high-affinity cell surface cAMP receptor CAR1, and k_i are the kinetic parameters. In the model, pulses of cAMP are produced when ACA is activated after the binding of extracellular cAMP to the surface receptor CAR1. When cAMP accumulates internally, it activates the protein kinase PKA. Ligand-bound CAR1 also activates the MAP kinase ERK2. ERK2 is then inactivated by PKA and no longer inhibits the cAMP phosphodiesterase REG A. A protein phosphatase activates REG A such that REG A can hydrolyse internal cAMP. When REG A hydrolyses the internal cAMP, PKA activity is inhibited by its regulatory subunit, and the activities of both ACA and ERK2 go up. Secreted cAMP diffuses between cells before being degraded by the secreted phosphodiesterase PDE [13, 16].

Details of the kinetic parameters are given in Table I. Figure 1(a) depicts the interactions between the various proteins involved in the network. In the figure, the arrow $\rightarrow$ indicates activation and $\dashv$ indicates deactivation. As can be seen from the figure, the proposed network comprises a number of interacting positive and negative feedback control loops, which together give rise to stable oscillations, as shown in Figure 1(b). Note that, as discussed in [13], the amplitudes, periods, and phase relations between the different oscillating states of the model match well with the available experimental data.

Table I. Nominal parameters.

Parameters	Nominal value	Parameters	Nominal value
k_1 (1/min)	2.0	k_8 (1/μM min)	1.3
k_2 (1/μM min)	0.9	k_9 (1/min)	0.3
k_3 (1/min)	2.5	k_{10} (1/μM min)	0.8
k_4 (1/min)	1.5	k_{11} (1/min)	0.7
k_5 (1/min)	0.6	k_{12} (1/min)	6.9
k_6 (1/μM min)	0.8	k_{13} (1/min)	23.0
k_7 (μM min)	1.0	k_{14} (1/min)	4.5

2.2. Structured singular value μ

In this paper, the structured singular value, denoted by μ, is used to analyse the robustness of the network model described above. The structured singular value [8, 10, 16] is defined as follows:

$$\frac{1}{\mu} := \min_{\Delta} \{\bar{\sigma}(\Delta) \,|\, \det(I - M(\mathrm{j}\omega)\Delta) = 0 \text{ for } \Delta \in B_\Delta\}$$

where $\bar{\sigma}(\cdot)$ denotes the maximum singular value, $M(\mathrm{j}\omega)$ the transfer function of a linear time invariant system, and B_Δ is a set of admissible norm-bounded uncertainties. In standard robust control theory, the structured singular value is usually understood as the smallest possible uncertainty, which makes the system unstable. In this paper, however, the nominal oscillating system has an unstable steady state, and thus μ can be interpreted as the smallest perturbation that makes the system stable, i.e. which destroys the oscillation [18]. The unstable steady state of the model (1) is computed as follows:

$$x^* = (2.4325, 1.6226, 0.8210, 0.9370, 0.9735, 0.3475, 1.7761)$$

Using this equilibrium point, we can linearize the model as follows:

$$\Delta\dot{x} = A\Delta x \tag{2}$$

DOI: 10.1002/rnc

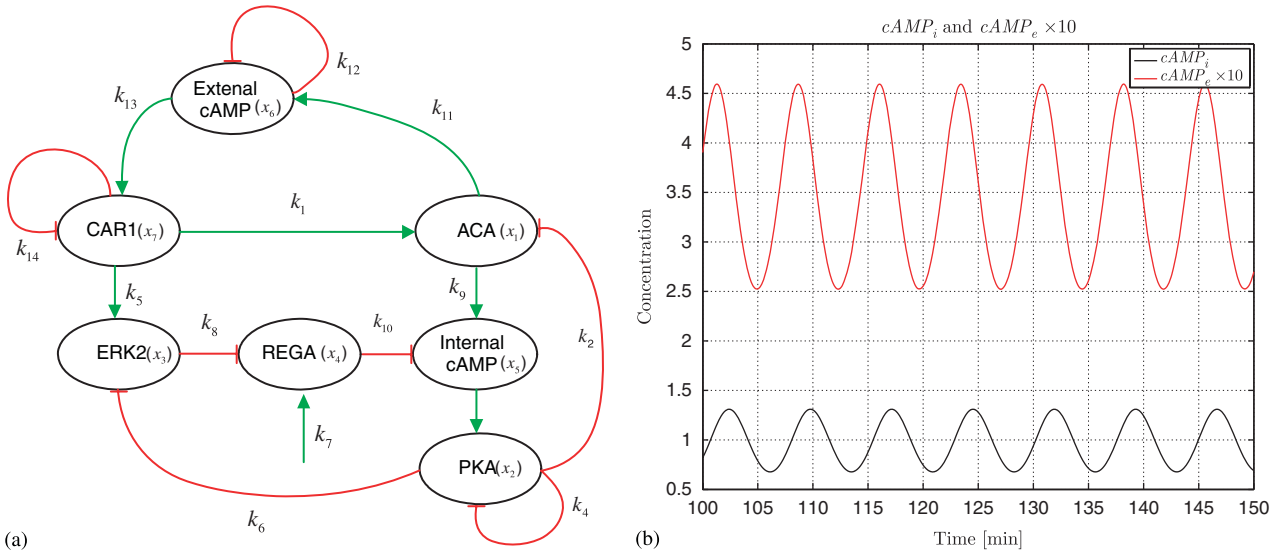

Figure 1. Original biochemical network model for cAMP oscillations in *Dictyostelium*. (a) Schematic diagram of the original network model and (b) internal and external cAMP oscillations (arbitrary units).

where $\Delta x = x - x^*$ and the matrix A is the Jacobian of the model (1) computed at the equilibrium x^*. Thus, the linearized model (2) is given as follows:

$$\Delta\dot{x} = \begin{bmatrix} -k_2x_2 & -k_2x_1 & 0 & 0 & 0 & 0 & k_1 \\ 0 & -k_4 & 0 & 0 & k_3 & 0 & 0 \\ 0 & -k_6x_3 & -k_6x_2 & 0 & 0 & 0 & k_5 \\ 0 & 0 & -k_8x_4 & -k_8x_3 & 0 & 0 & 0 \\ k_9 & 0 & 0 & -k_{10}x_5 & -k_{10}x_4 & 0 & 0 \\ k_{11} & 0 & 0 & 0 & 0 & -k_{12} & 0 \\ 0 & 0 & 0 & 0 & 0 & k_{13} & -k_{14} \end{bmatrix}$$

$$= \begin{bmatrix} -1.4603 & -2.1893 & 0 & 0 & 0 & 0 & 2.00 \\ 0 & -1.5000 & 0 & 0 & 2.5000 & 0 & 0 \\ 0 & -0.6568 & -1.2981 & 0 & 0 & 0 & 0.60 \\ 0 & 0 & -1.2181 & -1.0673 & 0 & 0 & 0 \\ 0.30 & 0 & 0 & -0.7788 & -0.7496 & 0 & 0 \\ 0.70 & 0 & 0 & 0 & 0 & -4.90 & 0 \\ 0 & 0 & 0 & 0 & 0 & 23.00 & -4.50 \end{bmatrix} \Delta x = A\Delta x$$

Note that it can be seen easily that the equilibrium is unstable in light of the eigenvalues of the A matrix,

DOI: 10.1002/rnc

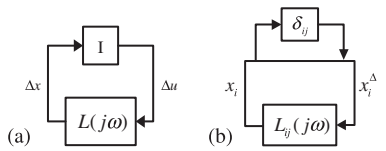

Figure 2. Perturbation between network interactions: (a) nominal network and (b) perturbed network.

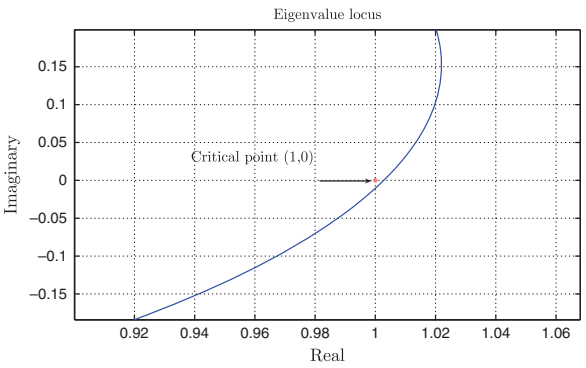

Figure 3. Eigenlocus of $L(\mathrm{j}\omega)$, $\omega \in [0, \infty]$.

$0.0042 \pm \mathrm{i}0.8570$. Using this linearized model and applying the structured singular value, we now identify the most fragile parts of the model, as described in the next subsection.

2.3. *Identifying fragile channels in the model*

In this subsection, we apply the approach proposed in [12] to the model (1) in order to identify the most fragile parts of the biochemical network from a structural point of view. These points in the network can then be examined, in the light of results from the experimental literature, to see whether there exist other interactions whose dynamics can be added to the model. In the linearized model (2), the off-diagonal elements of the matrix A indicate the interactions between the different components in the biochemical network. To see more clearly how these interactions affect the dynamic behaviour of the network, the linearized model can be written as

$$\Delta\dot{x} = \tilde{A}\Delta x + (A - \tilde{A})\Delta u \tag{3}$$

where $\tilde{A}$ is a diagonal matrix whose diagonal elements are those of the matrix A. Then, the transfer function of the linearized model (3) from Δu to Δx is given by

$$L(\mathrm{j}\omega) = (\mathrm{j}\omega I - \tilde{A})^{-1}(A - \tilde{A})$$

Note that the transfer function $L(\mathrm{j}\omega)$ is a 7×7 transfer function matrix and that the original interactions are recovered with $\Delta u = \Delta x$ as in Figure 2(a). Figure 3 shows the eigenlocus of the transfer function $L(\mathrm{j}\omega)$ with respect to the frequency ω. We can see that the eigenlocus is quite close to the critical point $+1$. In view of the generalized Nyquist stability criterion and Figure 3, it is clear that a small perturbation could make the eigenlocus move towards and finally encircle the critical point $+1$, which would correspond to the disappearance of the oscillation. In order to study robustness against such perturbations in a quantitative manner, we consider the perturbed network as shown in Figure 2(b). By looking into the smallest δ_{ij} which changes the stability of the equilibrium from unstable to stable, we can see how the model is robust against dynamic perturbations in the interaction between different components in the network. In particular, we are interested in perturbing interactions between two components in the network for the purpose of finding structurally fragile channels. To this end, we consider a perturbation $\delta_{ij}(\mathrm{j}\omega)$ for an element L_{ij} of the transfer function $L(\mathrm{j}\omega)$, where $L_{ij}(\mathrm{j}\omega)$ denotes the element in the ith row and jth column of the transfer function matrix $L(\mathrm{j}\omega)$. Then, the perturbed form of the element $L_{ij}(\mathrm{j}\omega)$ in the transfer function $L(\mathrm{j}\omega)$ can be written as:

$$L_{p,ij}(\mathrm{j}\omega) = L_{ij}(\mathrm{j}\omega)(1 + \delta_{ij}(\mathrm{j}\omega)) \tag{4}$$

Figure 4 shows the smallest δ_{ij} for each network channel which makes the network stable. Note that we take only existing interactions from Figure 1 into account. In Figure 4, δ_{ij} denotes the influence of the jth component on the ith component. Note in particular the value of δ_{17}, which is extremely small compared with the others. This extremely small stabilizing perturbation indicates a fragile point in the structure of the network [11, 12], and motivates us to investigate whether there are other modules that could be added to the original model between x_1 (ACA) and x_7 (CAR1) to improve the structural robustness of the

DOI: 10.1002/rnc

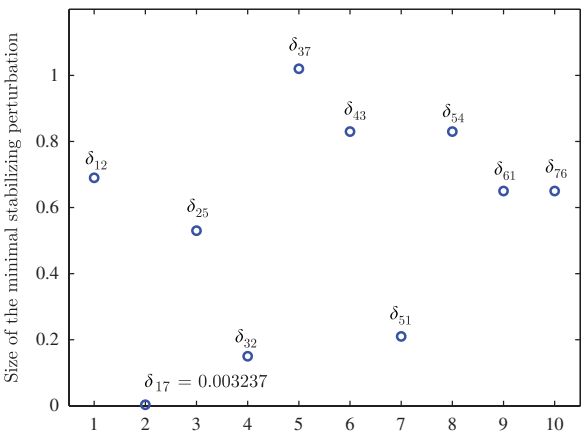

Figure 4. Minimal stabilizing perturbation.

model at this point. In fact, an analysis of the available data from the experimental literature confirms that the original model neglects important interactions between certain of the proteins in the network and Ca^{2+} and IP_3, and that these interactions occur at the most fragile part of the original network, as discussed in the following section.

3. EXTENSION OF THE MODEL

In this section, we briefly describe the extension of the original model based on the robustness analysis results of the previous section and an analysis of the available experimental data on *Dictyostelium* signalling mechanisms. It has been shown experimentally that the levels of intracellular Ca^{2+} and cAMP in *Dictyostelium* are tightly interconnected ([19] and references therein). Based on these experimental results, we have considered cAMP production and degradation to be dependent on the level of intracellular Ca^{2+}, which in turn is determined by a balance of fluxes into the cytoplasm from extracellular medium and endoplasmic reticulum (ER) and fluxes mostly generated by the membrane pumps compensating Ca^{2+} leaks across the plasma and ER membranes. IP_3 is synthesized by the Ca^{2+}-dependent and G protein-dependent phospholipase C (PLC). IP_3 concentration also has a major impact on the Ca^{2+}-dependent IP_3 receptor (IP_3R) located on the ER membrane. To take account of the above effects, the molecular circuit regulating the production of cAMP oscillations in *Dictyostelium* has been modelled as three interconnected modules involving intracellular Ca^{2+}, IP_3, and the G protein-coupled receptor cAR1, as shown in Figure 5. When external cAMP binds to cAR1, the G-protein cascade activates intracellular ACA. Transiently activated cAR1 can also lead to the activation of ACAs via the MAP kinase (ERK2). Intracellular cAMP is produced by ACA and degraded by intracellular phosphodiesterase (RegA). ERK2 is inhibited by cAMP-dependent PKA. Inactivated ERK2 loses its ability to phosphorylate RegA, in turn boosting the level of RegA activity. cAMP release creates an extracellular feedback loop for the cell, and also provides a source of additional cAMP signals for other cells in the vicinity. In addition to diffusion, the external cAMP feedback loop is also diminished by the externalPDE.

The network responsible for Ca^{2+} oscillations in *Dictyostelium* constitutes two feedback mechanisms. The first feedback loop is based on the movement of Ca^{2+} ions between the ER and cytoplasm. Intracellular Ca^{2+} is sequestered into the ER by sarco/ER Ca^{2+}-ATPase. It is released from the ER back into the cytoplasm via the IP_3R (which has both a Ca^{2+} and IP_3 dependence), as well as by a direct leak through the ER membrane. Another feedback mechanism involves the Ca^{2+} release from the intracellular compartment into the extracellular space by a plasma membrane Ca^{2+} pump (PMCA). PMCA compensates for the constant Ca^{2+} leak throughout the surface of the plasma membrane into the intracellular space. Other routes of Ca^{2+} into the cytoplasm include a range of Ca^{2+} channels, including the stretch-activated Ca^{2+} channels that play a particularly important role in *Dictyostelium* chemotaxis via the directed migration mechanism. IP_3 is produced by the only PLC isoform found in *Dictyostelium*, which is structurally similar to the mammalian isoform and regulated by both Ca^{2+} and G-protein pathways. IP_3 is further converted into IP4 by IP_3 kinase (IP_3K).

The intracellular Ca^{2+} regulation network described above is directly connected in the extended model with the G protein-coupled pathways included in the original model of Laub and Loomis [13]. Figure 6(a) describes

DOI: 10.1002/rnc

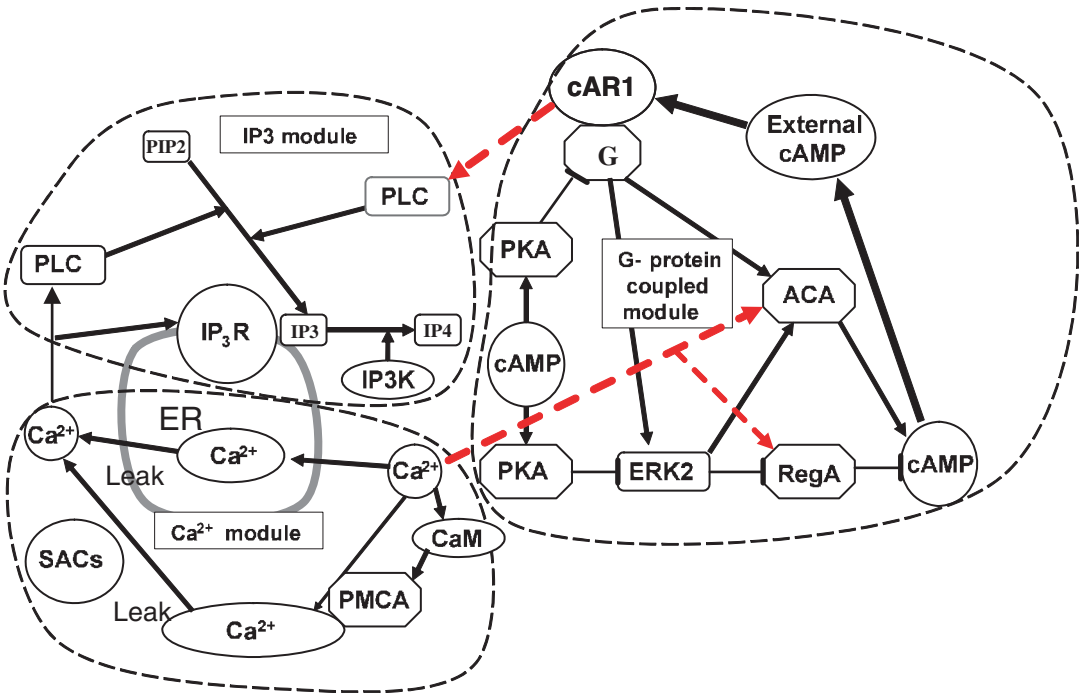

Figure 5. Details of the extended model.

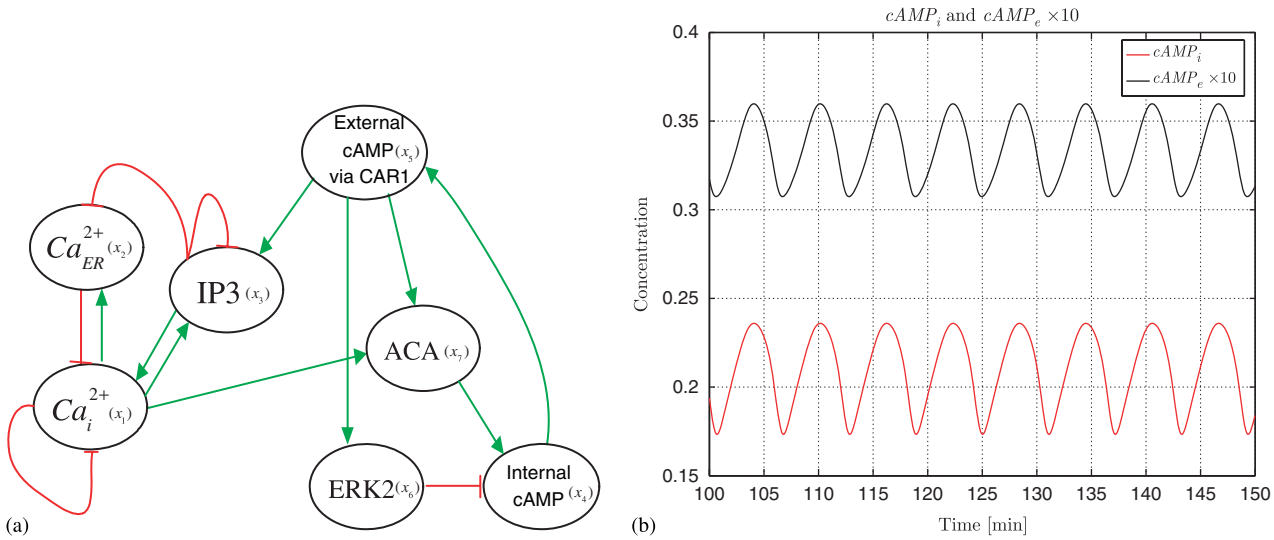

Figure 6. Extended biochemical network model for cAMP oscillations in *Dictyostelium*. (a) Schematic diagram of the extended network model and (b) internal and external cAMP oscillations in the extended model (arbitrary units).

DOI: 10.1002/rnc

the structure of the extended model, which comprises the following set of nonlinear differential equations:

$$\frac{dx_1}{dt} = j_{PM}^{in}\cdot\left(\psi_i - 0.5\cdot\ln\left(\frac{Ca_{out}^{2+}}{x_1}\right)\right) - j_{PM}^{A}\cdot\frac{x_1}{k_a^i + x_1}\cdot\frac{CaMx_1}{k_{CaM}+CaMx_1} + j_{ER}^{in}\cdot p_{ER}^{Ca^{2+}}\cdot x_2 - a_4\cdot p_{ER}^1\cdot p_{ER}^2$$

$$\frac{dx_2}{dt} = \frac{V_i - V_{ER}}{V_{ER}}\cdot(-j_{ER}^{in}\cdot p_{ER}^{Ca^{2+}}\cdot x_2 + a_4\cdot p_{ER}^1\cdot p_{ER}^2)$$

$$\frac{dx_3}{dt} = \mu_{PLC_{Ca^{2+}}}\cdot\frac{{x_1}^4}{(k_{Ca^{2+}}+x_1)^4} + \mu_{PLC_G}\cdot\frac{x_5}{k_G+x_5} + ap - \mu_{IP_3K}\cdot\frac{x_3}{k_{ip}+ip3}$$

$$\frac{dx_4}{dt} = D_{x_7}\cdot ACA* - RegA_i\cdot\frac{x_4}{k_{RegA}+x_4}\cdot\frac{k_{ER}}{k_{ER}+x_2} - K_{out}^{cAMP}\cdot\frac{{x_4}^2}{(k_{cAMP}+x_4)^2} - K_{out}^{Ca^{2+}}\cdot\frac{x_1}{k_{Ca^{2+}}+x_1}$$

$$\frac{dx_5}{dt} = K_{out}^{cAMP}\cdot\frac{{x_4}^2}{(k_{cAMP}+x_4)^2}\cdot(x_4 - x_5) + K_{out}^{Ca^{2+}}\cdot\frac{x_1}{k_{Ca^{2+}}+x_1} - PDE_e\cdot\frac{x_5}{k_{PDE}+x_5}$$

$$\frac{dx_6}{dt} = d_1\cdot\left(\frac{PKA}{c_1}\cdot(1-x_6) - x_6\right)$$

$$\frac{dx_7}{dt} = d_2\cdot\left(\frac{PKA}{c_2}\cdot(1-x_7) - x_7\right) \quad (5)$$

where x_1 is Ca_i^{2+}, x_2 is Ca_{ER}^{2+}, x_3 is IP_3, x_4 is $cAMP_i$, x_5 is $cAMP_e$, x_6 is ERK_2, and x_7 is ACA. Note that, due to their almost linear dependence on other states, the variables PKA, RegA, and CAR1 in the original model have not been included as independent states in the extended model, but appear implicitly in the equations, in order to keep the complexity of the extended model within manageable levels. Owing to space limitations, we do not present here a full description of the derivation of the extended model equations given above, or of the meaning of all of the model parameters—the interested reader is referred to [20] for full details of the model and the underlying experimental results. The key point to be noticed about the extended model for our purposes is that, as shown in Figure 6(a), the newly added modules in the extended model are connected at the point of interaction between the states x_1(ACA) and x_7(CAR1) in the original model, i.e. at the exact point of fragility in the original network revealed by our structural robustness analysis. As shown in Figure 6(b), the nominal responses of the extended model also generate stable oscillations, and match well with the experimental data. The obvious question that now arises is whether the extended model exhibits improved robustness characteristics when compared with the original 'minimal' model—this issue is addressed in the following section.

4. COMPARING THE ROBUSTNESS PROPERTIES OF THE EXTENDED AND ORIGINAL MODELS

In this section, we compare the robustness of the oscillations produced by the original and extended models against variations in a set of parameters that are common to both models. In particular, we are interested in the effects of parametric uncertainty on

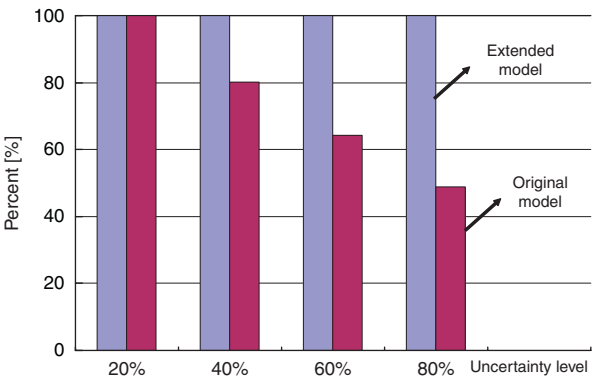

Figure 7. Robustness comparison: existence of stable oscillations.

DOI: 10.1002/rnc

Table II. Robustness test.

	Original model		Extended model	
	Period (min)	Amplitude	Period (min)	Amplitude
20% perturbation	Mean: 11.12 STD: 0.50 100% oscillation	Mean: 0.62 STD: 0.11	Mean: 9.09 STD: 0.02 100 % oscillation	Mean: 0.63 STD: 0.09
40% perturbation	Mean: 11.60 STD: 0.93 19.8% no oscillation	Mean: 0.64 STD: 0.12	Mean: 9.10 STD: 0.05 100% oscillation	Mean: 0.67 STD: 0.21
60% perturbation	Mean: 12.12 STD: 1.42 35.8% no oscillation	Mean: 0.62 STD: 0.13	Mean: 9.12 STD: 0.11 100% oscillation	Mean: 0.72 STD: 0.34
80% perturbation	Mean: 12.08 STD: 1.38 51.2% no oscillation	Mean: 0.62 STD: 0.13	Mean: 9.26 STD: 0.94 100% oscillation	Mean: 0.73 STD: 0.45

the amplitude, period, and stability of the oscillations. We focus on uncertainties in a set of parameters that determine the dynamics of the extracellular cAMP positive feedback loop in both models—these are k_9, k_{10}, k_{11}, and k_{12} in the original model and D_{ACA}, RegA_i, $K_{\mathrm{out}}^{\mathrm{cAMP}}$, and PDE_e in the extended model. To compare the robustness of the two models we carry out 1000 Monte Carlo simulations for a number of different uncertainty levels, in which the sample value for each parameter is drawn from the set:

$$p = \bar{p}(1+\varepsilon\cdot\delta) \tag{6}$$

where p denotes the sampled value of the parameter used in the simulation, $\bar{p}$ is the nominal value of the parameter, ε is the maximal level of the perturbation (chosen as 0.2, 0.4, 0.6, and 0.8 in the various Monte Carlo simulation campaigns), and δ is a uniformly distributed random number between -1 and 1. Figure 7 shows that the percentage of simulations producing stable oscillations falls dramatically for the original model as the maximum allowable level of uncertainty in the kinetic parameters is increased. For the extended model, however, 100% of the simulations produce stable oscillations even for the highest level of uncertainty, demonstrating a dramatic improvement in the robustness of the model. In Table II, the effect of the uncertainty on the period and amplitude of the oscillations is reported for each model. The standard deviation of the periods for each different level of uncertainty is approximately an order of magnitude smaller in the case of the extended model, even though the standard deviation is calculated only for the cells displaying stable oscillations in each case. Note also that although the standard deviations of the amplitudes appear to be similar for both models, in reality there is a much greater level of variation in the amplitudes of the original model. This is because the standard deviations are calculated only for those cells displaying stable oscillations in each case, and it is precisely those cells that are no longer generating stable cAMP oscillations which have the largest deviation from the nominal amplitude values.

5. CONCLUSIONS

In this paper we showed how techniques from robust control theory could be used to analyse and extend a mathematical model of the interacting proteins underlying cAMP oscillations in aggregating *Dictyostelium* cells. Starting with a previously proposed 'minimal' model, we showed how robustness analysis using the structured singular value can identify points of structural fragility in the network. By combining these

DOI: 10.1002/rnc

results with insights from recent results from the experimental literature, we showed how the original model can be augmented with some important additional modules, comprising networks involving IP_3 and Ca^{2+}, which interact with the original model at precisely the points of fragility identified via our initial robustness analysis. A comparative analysis of the two models revealed dramatic improvements in robustness against uncertainty in a set of parameters common to both networks, thus confirming the key role of dynamic interactions between the different modules in generating robust cAMP oscillations. The results of our study highlight the usefulness of robustness analysis techniques in validating and improving mathematical models of biochemical networks.

ACKNOWLEDGEMENTS

This work was supported by BBSRC research grant BB/D015340/1. This work was also supported by the National Research Foundation of Korea (NRF) grant funded by the Korea Ministry of Education, Science & Technology (MEST) through the BRL (Basic Research Laboratory) grant (2009-0086964), the Systems Biology grant (20090065567), the Nuclear Research grant (M20708000001-07B0800-00110), the 21C Frontier Microbial Genomics and Application Center Program (Grant MG08-0205-4-0), and the WCU grant (R32-2008-000-10218-0). This work was also supported by the 'Systems biology infrastructure establishment grant' provided by Gwangju Institute of Science & Technology in 2009.

REFERENCES

1. Kitano H. Biological robustness. *Nature Reviews Genetics* 2004; **5**:826–837.
2. Stelling J, Sauer U, Szallasi Z, Doyle FJ, Doyle J. Robustness of cellular functions. *Cell* 2004; **118**:675–685.
3. Ma L, Iglesias PA. Quantifying robustness of biochemical network model. *BMC Bioinformatics* 2002; **3**(38):1471–2105.
4. Carlson JM, Doyle J. Complexity robustness. *Proceedings of the National Academy of Sciences* 2002; **99**:2538–2545.
5. Stelling J, Gilles ED, Doyle FJ. Robustness properties of circadian clock architectures. *Proceedings of the National Academy of Sciences* 2004; **101**(36):13210–13215.
6. Kwon Y-K, Cho K-H. Quantitative analysis of robustness and fragility in biological networks based on feedback dynamics. *Bioinformatics* 2008; **24**(7):987–994.
7. Kim J-R, Yoon Y, Cho K-H. Coupled feedback loops form dynamic motifs of cellular networks. *Biophysical Journal* 2008; **94**(2):359–365.
8. Doyle JC. Analysis of feedback systems with structured uncertainties. *IEE Proceedings*, *Part D* 1982; **129**: 242–250.
9. Zhou K, Doyle JC. *Essentials of Robust Control*. Prentice-Hall: Englewood Cliffs, NJ, 1997.
10. Skogestad S, Postlethwaite I. *Multivariable Feedback Control*. Addison-Wesley: Reading, MA, 2005.
11. Morohashi M, Winn AE, Borisuk MT, Bolouri H, Doyle J, Kitano H. Robustness as a measure of plausibility in models of biological networks. *Journal of Theoretical Biology* 2002; **216**:19–30.
12. Jacobsen EW, Cedersund G. Structural robustness of biochemical network models with application to the oscillatory metabolism of activated neutrophils. *IET Systems Biology* 2008; **2**(1):39–47.
13. Laub MT, Loomis WF. A molecular network that produces spontaneous oscillations in excitable cells of Dictyostelium. *Molecular Biology of the Cell* 1999; **9**: 3521–3532.
14. Fache S, Dalous J, Engelund M, Hansen C, Chamaraux F, Fourcade B, Satre M, Devreotes P, Bruckert F. Calcium mobilization stimulates Dictyostelium discoideum shear-flow-induced cell motility. *Journal of Cell Science* 2005; **118**: 3445–3457.
15. Williams RS, Boeckeler K, Graf R, Muller-Taubenberger A, Li Z, Isberg RR, Wessels D, Soll DR, Alexander H, Alexander S. Towards a molecular understanding of human diseases using Dictyostelium discoideum. *Trends in Molecular Medicine* 2006; **12**:415–424.
16. Kim J, Bates DG, Postlethwaite I, Ma L, Iglesias PA. Robustness analysis of biochemical network models. *IEE Proceedings—Systems Biology* 2006; **153**(3):96–104.
17. Kim J, Heslop-Harrison P, Postlethwaite I, Bates DG. Stochastic noise and synchronisation during Dictyostelium aggregation make cAMP oscillations robust. *PLoS Computational Biology* 2007; **3**(11):e218.
18. Schmidt H, Jacobsen EW. Identifying feedback mechanisms behind complex cell behaviors in biochemical networks. *IEEE Control Systems Magazine*, *Special Issue*: *Systems Biology* 2004; **24**(4):91–102.
19. Lusche DF, Bezares-Roder K, Happle K, Schlatterer C. cAMP controls cytosolic Ca^{2+} levels in Dictyostelium discoideum. *BMC Cell Biology* 2005; **6**:12.
20. Valeyev NV, Kim J-S, (Pat) Heslop-Harrison JS, Postlethwaite I, Kotov NV, Bates DG. Computational modelling suggests dynamic interactions between Ca^{2+}, IP_3 and G protein-coupled modules are key to robust Dictyostelium aggregation. *Molecular BioSystems* 2009; **15**: 612–628.

DOI: 10.1002/rnc